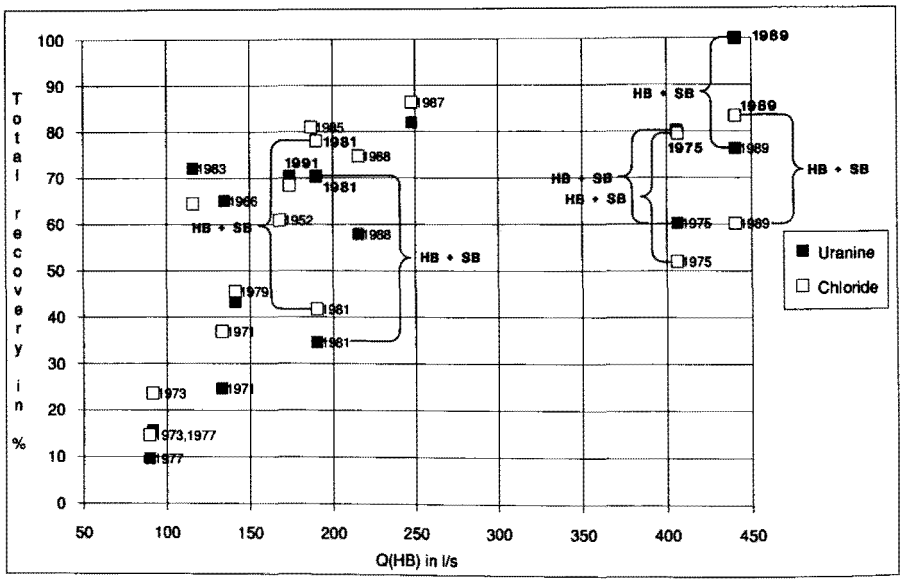

Fig. 5.13: Correlation diagramm of discharges of the Hammerbach spring and the total tracer recoveries for uranine and chloride at Hammerbach and Schmelzbach spring of all tracing experiments with injections into the Lurbach sinkhole.

quaternary filling in the Mur valley (cf. chap. 2.3.5. and 2.3.6.). Therefore the percentage of tracer losses is higher at low water conditions.

The transit times of the tracer uranine (expressed by the concentration peak in h after injection) between the Lurbach sinkhole and the Hammerbach spring as function of the mean discharge of the spring (and discharge extreme values during the experiments) are plotted in fig. 5.14. The exponential function indicates that the residence time in the karst aquifer depends significantly on the spring discharge and varies between 19 h (experiment 1975 at high water conditions) and 75 h (experiment 1973 with the lowest discharges). The experiments with tracer detection also in Schmelzbach are marked separately in fig. 5.14. It is clearly visible that the overflow from Hammerbach to Schmelzbach aquifer is only active at higher discharges.

6. Application of Tracer Models

6.1. Mathematical Modelling of Tracer Experiments in the Karst of Lurbach System (P. MALOSZEWSKI, T. HARUM, R. BENISCHKE)

6.1.1. Introduction

Water storage and water flow in karstic groundwater systems focus a lot of attention, especially in the countries where drinking water is mainly obtained from the karst. The estimation of the water volume in the karstic catchment areas and the prediction of protection zones against contamination in the surrounding of those

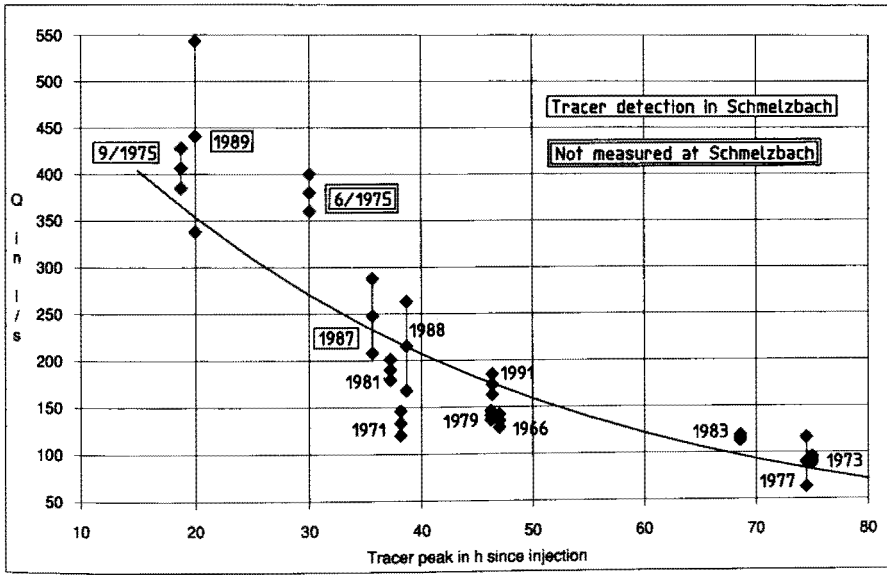

Fig. 5.14: Correlation diagramm of discharges of the Hammerbach spring and the transit time (tracer concentration peak in h since injection) for uranine at Hammerbach spring of calculated from all tracing experiments with injections into the Lurbach sinkhole.

areas play then a very important role. Experimental works in the karst are mainly based on classical hydraulic methods in which the parameters are obtained from analysing the recharge-discharge relations (S. DREISS, 1989, Th. PFAFF, 1987).

For several years the applicability of environmental and artificial tracer methods has been permanently increasing (R. BENISCHKE et al, 1988, D. RANK et al, 1991, J.-F. QUINLAN et al, 1987). Especially artificial tracer experiments have been already widely applied. Several well described tracer experiments performed in karst of different types can be found in the literature (W. KÄSS, 1972, R. GOSPODARIC & P. HABIČ, 1976, R. GOSPODARIČ et al., 1976, H. BEHRENS et al., 1981, A. MORFIS & H. ZOJER, 1986). In most cases the purpose of these experiments was the determination of flow directions and/or hydraulic connections between injection and detection sites. Unfortunately only some of these experiments have been interpreted quantitatively. The interpretation is usually mostly based on the method of moments (A. KREFT & A. ZUBER, 1978) applied directly to the tracer concentration curve or on a simple one dimensional dispersion model developed for porous aquifers by A. LENDA & A. ZUBER (1970).

It means that in most cases the transport parameters such as water velocity (mean transit time of tracer) and dispersivity are being determined without model calibration or by calibration of an unadequate model, because the tracer concentration curves in karst are characterized by strong tailing effect and often by several peaks.

As shown by P. MALOSZEWSKI & A. ZUBER (1990, 1992) the method of moments applied to the tracer breakthrough curves characterized by tailing effect provides a strong overestimation of longitudinal dispersivity and underestimation of water velocity. The dispersivities obtained in this way range from hundred of meters to

kilometers (I. STOBER, 1988). Additionally these parameters used in one dimensional dispersion model yield the tracer breakthrough curve far from the concentrations measured. Even by applying the fitting procedure, the simple one dimensional model cannot fit the tracer concentration curve correctly. This means that the model is not calibrated properly and, consequently, not validated (s. P. MALOSZEWSKI & A. ZUBER, 1992, for the definition of these terms).

Three approaches have been proposed so far to deal with the tailing effect. The first consists of coupling of the dispersion equation for mobile water in conduit fractures with the diffusion equation for stagnant water in the microporous matrix (P. MALOSZEWSKI & A. ZUBER, 1985). The second consists of considering the tracer curve as a result of superposition of several flow paths (A. ZUBER, 1974, A. KREFT et al., 1974) and also different flow paths in series (R. ROGALSKI, 1988). The third is the combination of both above approaches (P. MALOSZEWSKI & A. ZUBER, 1985, K.-P. SEILER et al., 1989). In the present work the second approach is employed and further developed for modelling tracer transport in the karstic system of Lurbach.

6.1.2. Mathematical Concept

Most tracer experiments were performed in the karst of Lurbach system under quasi steady state conditions, i.e., the discharge of the Hammerbach spring was nearly constant during the tracer passage. The tracers were injected directly into the Lurbach creek entering the karstic system in a sinkhole and observed in two karstic outflows: Hammerbach and Schmelzbach springs (s. chap. 5.). All the tracer curves observed were characterized by strong tailing effects or even by additional peaks. Such effects cannot be described only by single one dimensional dispersion model. The determination of transport parameters using any simple estimation method without model calibrations cannot yield acceptable results. The shape of the tracer curves suggested that the tracer is transported in several parallel flow paths (subsystems). The idea of the tracer transport is shown in fig. 6.1. R. ROGALSKI (1988) employed a model consisting of two parallel flow paths, whereas here up to five were possible.

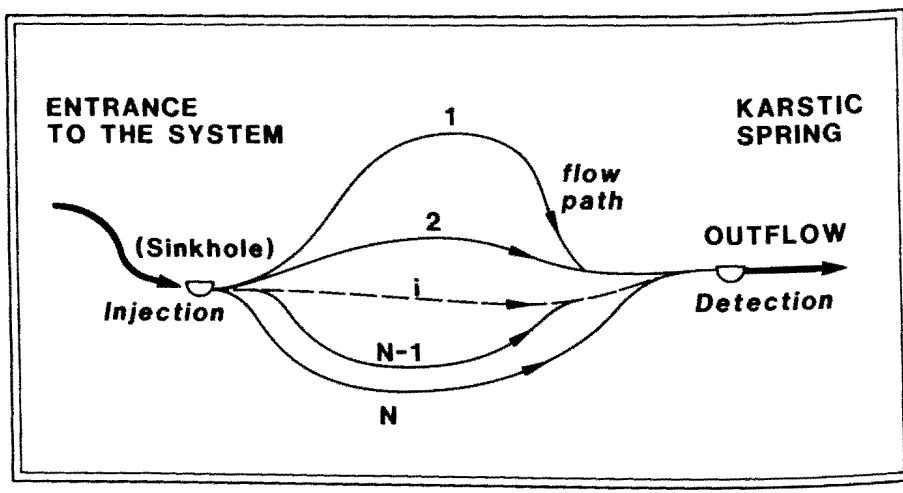

Fig. 6.1: Hydrological model of the water flow through drainage channels in the karstic system.

A similar multiflow model was presented by A. ZUBER (1974) and used by A. KREFT et al. (1974) for interpreting tracer experiments in fractured karstified rocks. In the present work this approach is employed to karstic conduits. It is assumed that the tracer transport can be considered separately for each flow path and that there are no interactions between the flow paths. Possible diffusion of tracer from the mobile water into the stagnant water in the microporous matrix and/or in temporarily nonactive parts of the karstic system is neglected. Under these assumptions on each parallel flow path the transport of an "ideal" (nonreactive) tracer is governed by a one dimensional dispersion model:

$$D_i \frac{\partial^2 C_i}{\partial x^2} + v_i \frac{\partial C_i}{\partial x} = \frac{\partial C_i}{\partial t}, \qquad (6.1)$$

where $C_i(x,t)$is the concentration of tracer in water, v_i is the mean water velocity, and D_i is the dispersion coefficient for the i-th flow path. The molecular diffusion in water in the comparison to the hydrodynamic dispersion is negligible due to high water velocities. The dispersion coefficient is then

$$D_i = \alpha_i v_i, \qquad (6.2)$$

where α_i is defined as the dispersivity on the i-th flow path.

The model assumes that the whole mass of tracer, M, instantaneously injected in time t = 0 at the entrance to the system, is there well mixed and divided into N portions which immediately enter the N flow subsystems. This means that the tracer mass M_i entering each subsystem is proportional to the volumetric flow rate Q_i through that subsystem. All the flow paths meet again in the outflow from the system (spring) where instantaneous good mixing of the tracer takes place. The conceptual flow model is shown in fig. 6.2. It is clear that in nature some flow paths may originate and end somewhere in the system (s. fig. 6.1), but not like shown in fig. 6.2. Independently from that, the model parameters are always related to flow paths which begin in the sinkhole (injection site) and end in the outflow from the system

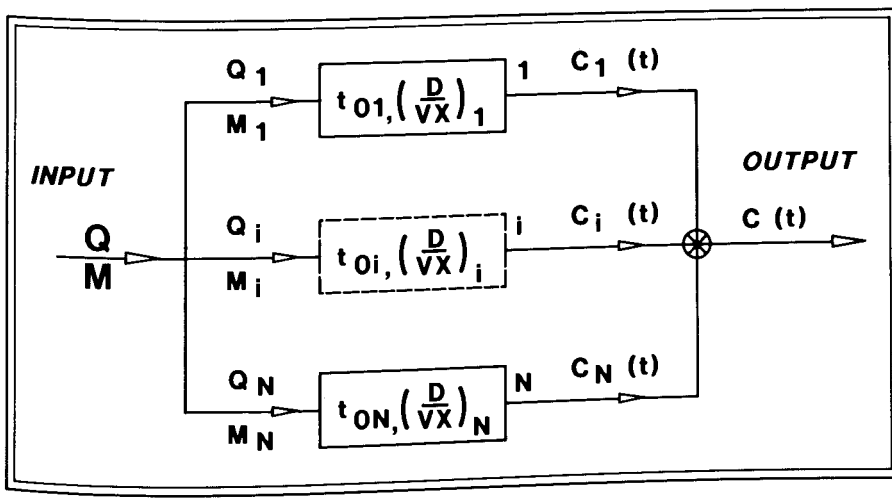

Fig. 6.2: The conceptual flow model.

(spring). **Due to this fact, the model has to be considered as a rough approximation of the reality.** The number of possible flow subsystems N is one of the parameters of the model and has to be determined during its calibration (fitting). The parameters of the model found from the tracer data strongly depend on the tailing part of the tracer concentration curve and the accuracy of its measurement. The flow distances, x_i, measured between the injection and detection site (sinkhole and spring, respectively) can be different for different flow paths and is not exactly known. Due to this fact it is always convenient to use as transport parameters: the mean transit time of water $t_0 = x/v$ and the dispersion parameter $D/vx = \alpha/x$. Assuming steady state flow conditions the mean transit time of water for the i-th flow path, t_{0i}, is simultaneously equal to the ratio of the volume of water V_i to the volumetric flow rate of water Q_i through the flow subsystem:

$$t_{0i} = x_i/v_i = V_i/Q_i \,. \tag{6.3}$$

For an instantaneous injection described by the Dirac function

$$C_i(0,t) = M_i/Q_i \cdot \delta(t) \tag{6.4}$$

the solution of eq. (6.1) has the following form:

$$C_i(t) = \frac{M_i}{V_i} \frac{1}{\sqrt{4\pi (D/vx)_i (t/t_{0i})^3}} \cdot \exp\left[-\frac{(1 - t/t_{0i})^2}{4 (D/vx)_i (t/t_{0i})}\right], \tag{6.5}$$

where

$$(D/vx)_i = \alpha_i/x_i \tag{6.6}$$

is the dispersion parameter on the i-th flow path.

The tracer concentration measured in the outflow from the system is the weighted mean concentration from all flow paths

$$C(t) = \sum_{i=1}^{N} [Q_i C_i(t)]/Q \,, \tag{6.7}$$

where $C_i(t)$ is the tracer output concentration at the end of the i-th flow path and Q is the total discharge measured in the karstic spring equal simultaneously to the sum of partial flow rates:

$$Q = \sum_{i=1}^{N} Q_i \,. \tag{6.8}$$

It can be deduced from eq. (6.7) that the tracer concentration $C_i(t)$ at the end of i-th flow path is diluted by other flow paths

$$C_{mi}(t) = Q_i C_i(t)/Q \,. \tag{6.9}$$

$C_{mi}(t)$ is now the tracer concentration from the i-th flow subsystem observed in the outflow from the whole system. Combining eq. (6.5) and (6.9) one obtains:

$$C_{mi}(t) = \frac{M_i}{Q} \frac{1}{t_{0i}\sqrt{4\pi (D/vx)_i (t/t_{0i})^3}} \cdot \exp\left[-\frac{(1 - t/t_{0i})^2}{4 (D/vx)_i (t/t_{0i})}\right]. \tag{6.10}$$

The total output concentration (eq. 6.7) is the superposition of the partial concentrations, $C_{mi}(t)$

$$C(t) = \sum_{i=1}^{N} C_{mi}(t) \,. \tag{6.11}$$

The theoretical tracer recovery R obtained in the outflow from the system is

$$R = Q \cdot \int_0^\infty C(t)\,dt\,, \tag{6.12}$$

whereas the partial tracer recoveries R_i observed at the end of each i-th flow path are calculated using the same equation but instead of Q and C(t) one has to use Q_i and $C_i(t)$. By introducing eq. (6.9) into (6.12) one obtains

$$R_i = Q \cdot \int_0^\infty C_{mi}(t) = M_i\,. \tag{6.13}$$

The mass of tracer injected into i-th flow path, M_i, can be then found using eq. (6.13) to the i-th tracer concentration curve measured in the outflow from the whole system. Theoretically the sum of all partial recoveries is equal to the total recovery and to the mass of tracer injected

$$R = \sum_{i=1}^{N} R_i = M\,. \tag{6.14}$$

The mathematical flow model for the Lurbach system is described by eq. (6.10) and (6.11).

The parameters of the model are the number of flow subsystems (N) and the parameters for each of the N flow paths. Each i-th flow path has its own mean transit time of water, t_{0i}, dispersion parameter, $(D/vx)_i$ and the flow rate, Q_i, represented by the mass of tracer, M_i.

6.1.3. Determination of the Parameters

The solution of the inverse problem, i.e. the determination of all parameters from the tracer curve cannot be done automatically due to the high number of unknowns. The solution can be obtained by dividing step by step the experimental curve into partial curves, starting by the first peak of the experimental curve and looking for the best fit of the theoretical solution (eq. 6.10) to the concentrations measured at the initial part of the curve. In the next step this theoretical curve is substracted from the whole tracer concentration curve and the procedure repeated until the background concentration is reached. The number of flow subsystems N will then be automatically found. As a result of fitting the parameters t_{0i} and $(D/vx)_i$ are determined step by step for all flow paths. The parameter M_i is estimated next, by applying eq. (6.13) to the partial theoretical curves calculated with known values of t_{0i} and $(D/vx)_i$. Finally, the whole theoretical curve can be calculated (eq. 6.11) and compared with the experimental curve.

In practice, the total recovery of tracer (eq. 6.12) is very often smaller than the mass injected (M). In such a case the real recoveries R_i have to be used instead of M_i in eq. (6.11) and (6.10).

Similarly, when the tracer curves are observed in several outflows from the karstic system, each single outflow must be separately considered and R used instead of M. The ratio of i-th recovery R_i to the total recovery R observed in the outflow produces the portion of tracer r_i transported through the i-th flow subsystem. According to the model assumption this quantity is equal to the ratio of volumetric flow rate in i-th flow path Q_i to the whole discharge Q of the outflow

$$r_i = R_i/R = Q_i/Q\,. \tag{6.15}$$

From the above equation it is clear that the estimation of the r_i parameter from the recoveries ratio enables to calculate the flow rates Q_i on each flow path (for known discharge Q) and then from eq. (6.3) the volumes of water V_i in different flow subsystems

$$V_i = Q_i \cdot t_{0i} = r_i \cdot Q \cdot t_{0i}. \tag{6.16}$$

The sum of V_i is equal to the whole water volume V in the drainage channels of the karstic system between the sinkhole of creek and its outflow

$$V = \sum_{i=1}^{N} V_i. \tag{6.17}$$

6.1.4. Results of Modelling and Discussion

It was mentioned earlier that the tracers were injected into the Lurbach creek (input) and observed in the outflows: Hammerbach and Schmelzbach springs (outputs). Twenty tracer experiments have been performed since 1927 – three experiments were not completed but 17 tracer concentration curves were sufficiently well recorded to be modelled. The tracer passage was detected mainly in Hammerbach spring (15 curves). Only at discharges of the Hammerbach spring higher than about 200 l/s, the tracer passage was also detected in Schmelzbach spring. This phenomen was observed in 1970, 1975, 1981, 1987 to 1989 experiments (s. chap. 5.2.) but only two of them (1981 and 1989) could be modelled. In 1988 a multitracer experiment with three "ideal" tracers uranine, bromide and eosin injected simultaneously was performed by the ATH-group. The tracer curves obtained for uranine and eosin have nearly the same shape as that for bromide. It shows that the strong tailing effect observed in the experiments was not a result of possible sorption or diffusion, but can well be explained by the flow conditions. In some experiments the water samples were collected not long enough to obtain the whole tracer curve and it was necessary to extrapolate the tailing parts. The discharge of Hammerbach spring was nearly constant during most of experiments (steady state conditions). However, the mean discharge was different from year to year (80–360 l/s). The results of modelling for Hammerbach and Schmelzbach drainage systems are summarized in tab. 6.1–6.9. The velocities and dispersivities on different flow paths were calculated assuming the same lenghts of the N flow paths x_i in each system separately (x = 3.1 km for Hammerbach and x = 3.0 km for Schmelzbach).

The model proposed in this study yields a good fit in all experiments. It means that the model was in all cases properly calibrated and that the idea of multiflow seems to be applicable for this system. The examples of model calculations for tracer experiments performed in 1952, 1979 and 1988 are shown in fig. 6.3–6.6. The final results of modelling can only be discussed for Hammerbach system. There are not sufficient data for the Schmelzbach system to make any general conclusions.

6.1.4.1. Flow Paths

In the Hammerbach system between three and five flow paths (flow subsystems) were found. It is questionable if five flow paths really exist because it is difficult to model the end parts of tracer curve due to low concentration, close to background. On the other hand, some experiments, particulary for low discharges, were ended too early and consequently the determination of all flow paths was not possible. However, the experiment with bromide and uranine in 1988 showed that up to five flow subsystems probably exist.

*Tab. 6.1: Results of calculations for Hammerbach system (tracers, mean transit times, dispersivities on different flow paths). FP1, FP2, FP3, FP4 and FP5 = mean flow path 1, 2, 3, 4 and 5; *) = tracer experiment was ended to early and the whole tracer curve was not available.*

Year	Tracer	Mean transit times t_{0i} (days)					Dispersivity α_i (m)				
		FP1	FP2	FP3	FP4	FP5	FP1	FP2	FP3	FP4	FP5
1952	Chloride	2.0	2.6	3.3			23.0	6.3	12.9	–	–
1971	Uranine	1.7	2.4	3.1	*)		25.0	16.5	16.5	–	–
1973	Uranine	3.3	4.5	*)			24.3	13.9	–	–	–
1977	Uranine	3.2	4.5	*)			20.5	28.3	–	–	–
1979	Uranine	2.0	2.6	3.4	4.6	–	20.6	6.6	23.2	13.6	–
1981	Uranine	1.5	2.0	2.9	4.4	–	15.5	32.0	37.0	39.3	–
1983	Uranine	2.8	3.6	5.0	*)		18.7	15.8	9.2	–	–
1985	Amidor.	1.8	2.5	3.2	4.1	5.4	12.7	19.0	7.5	20.0	15.0
1987	Uranine	1.6	2.2	3.0	4.4		20.1	13.3	31.2	37.8	
1988	Bromide	1.7	2.2	2.8	3.6	5.0	11.3	9.8	16.5	8.5	27.0
	Uranine	1.7	2.2	2.9	3.6	4.3	11.6	16.5	14.3	7.5	6.5
	Eosin	1.7	2.2	2.8	*)		12.0	12.8	11.0	–	–
1989	Uranine	0.9	1.3	1.8	2.4	3.5	27.0	27.5	26.0	30.0	40.0
1991	Uranine	1.9	2.5	3.3	4.3	6.6	18.0	22.0	20.0	22.0	30.0
	Chloride	1.8	2.4	3.2	4.3	6.0	15.5	17.5	19.5	22.0	30.0

*Tab. 6.2: Results of calculations for Hammerbach system (mean discharge during experiment, portion of tracer and mean partial volumetric flow rates for different flow subsystems). FP1, FP2, FP3, FP4 and FP5 = mean flow path 1, 2, 3, 4 and 5; *) = tracer experiment was ended to early and the whole tracercurve was not available; [b] = bromide; [c] = chloride; [u] = uranine; [e] = eosin.*

Year	Mean Q (l/s)	Portion of tracer r_i					Mean partial flow rates Q_i (l/s)				
		FP1	FP2	FP3	FP4	FP5	FP1	FP2	FP3	FP4	FP5
1952	170.0	0.82	0.09	0.09			139.4	15.3	15.3	–	–
1971	133.0	0.63	0.21	0.16	*)		83.8	27.9	21.3	–	–
1973	91.5	0.75	0.25	*)			68.6	22.9	–	–	–
1977	81.3	0.64	0.36	*)			52.0	29.3	–	–	–
1979	141.0	0.69	0.09	0.15	0.07	–	97.3	12.7	21.2	9.9	–
1981	195.0	0.43	0.35	0.15	0.07		83.9	68.3	29.3	13.7	–
1983	116.0	0.65	0.28	0.07	*)		75.4	32.5	8.1	–	–
1985	186.0	0.55	0.18	0.09	0.11	0.07	102.3	33.5	16.7	20.5	13.0
1987	200.0	0.53	0.23	0.17	0.07		106.0	46.0	34.0	14.0	
1988	182.0[b]	0.69	0.13	0.09	0.03	0.06	125.6	23.7	16.4	5.5	11.1
	182.0[u]	0.64	0.21	0.09	0.03	0.02	116.5	38.2	16.4	5.5	3.6
	182.0[e]	0.74	0.18	0.08	*)		134.7	32.8	14.6	–	–
1989	360.0	0.44	0.30	0.15	0.07	0.03	158.4	108.0	54.0	25.2	10.8
1991	185.0[u]	0.47	0.19	0.12	0.12	0.09	87.0	35.2	22.2	22.2	16.7
	185.0[e]	0.51	0.17	0.15	0.11	0.06	94.4	31.5	27.8	20.4	11.1

Tab. 6.3: Results of calculations for Hammerbach system (total volume of water in the system, mean partial volumes of water in different flow subsystems and mean water velocities of water). FP1, FP2, FP3, FP4 and FP5 = mean flow path 1, 2, 3, 4 and 5.

Year	Total V (10^3 m^3)	Mean partial water volumes V_i (10^3 m^3)					Mean water velocity v_i (m/h)				
		FP1	FP2	FP3	FP4	FP5	FP1	FP2	FP3	FP4	FP5
1952	31.3	23.3	3.5	4.4	–	–	65.8	49.6	39.4		
1971	23.7	12.4	5.8	5.5	–	–	75.0	54.2	41.7		
1973	28.7	19.7	9.0	–	–	–	38.5	28.4			
1977	24.3	12.9	11.4	–	–	–	40.3	28.5			
1979	29.6	16.8	2.7	6.1	4.0	–	64.6	49.8	38.0	28.1	
1981	35.9	14.3	9.2	7.5	4.9	–	83.3	64.6	44.4	29.2	
1983	32.1	18.3	10.4	3.4	–	–	45.4	35.4	27.5		
1985	39.6	15.9	7.2	4.6	7.4	5.8	71.1	52.1	39.9	31.3	23.9
1987	39.0	14.8	8.8	9.0	6.0		80.3	59.2	42.5	29.0	
1988	35.6	20.2	4.8	4.2	1.7	4.7	75.4	58.6	45.8	36.1	25.8
	33.9	18.4	8.1	4.3	1.8	1.4	76.3	57.5	44.5	35.5	30.0
	32.1	21.5	6.8	3.7	–	–	76.0	57.4	45.4		
1989	39.0	11.5	11.7	7.6	5.0	3.0	150.0	103.2	72.9	54.2	36.7
1991	43.7	14.3	7.8	6.6	8.3	6.7	64.6	50.0	37.5	28.8	20.8
	42.1	14.6	6.5	7.7	7.9	5.4	69.6	52.5	39.6	29.2	20.8

*Tab. 6.4: Results of calculations for Schmelzbach system (tracers, mean transit times, dispersivities on different flow paths). FP1, FP2, FP3, FP4 and FP5 = mean flow path 1, 2, 3, 4 and 5; *) = tracer experiment was ended to early and the whole tracercurve was not available.*

Year	Tracer	Mean transit times (days)					Dispersivity (m)				
		FP1	FP2	FP3	FP4	FP5	FP1	FP2	FP3	FP4	FP5
1981	Uranine	1.8	2.8	4.3	*)		50.0	55.0	42.0	–	–
1989	Uranine	1.0	1.6	2.4	4.2	0.7	49.4	39.5	42.0	60.0	3.7

*Tab. 6.5: Results of calculations for Schmelzbach system (mean discharge during experiment, portion of tracer and mean partial volumetric flow rates for different flow paths). FP1, FP2, FP3, FP4 and FP5 = mean flow path 1, 2, 3, 4 and 5; *) = tracer experiment was ended to early and the whole tracercurve was not available.*

Year	Mean Q (l/s)	Portion of tracer					Mean partial flow rates (l/s)				
		FP1	FP2	FP3	FP4	FP5	FP1	FP2	FP3	FP4	FP5
1981	112.0	0.39	0.32	0.29	*)		43.7	35.8	32.5	–	–
1989	152.0	0.52	0.23	0.13	0.11	0.02	79.0	35.0	19.8	15.2	3.0

Tab. 6.6: Results of calculations for Schmelzbach system (total volume of water in the system, mean partial volumes of water in different flow subsystems and mean water velocities of water). FP1, FP2, FP3, FP4 and FP5 = mean flow path 1, 2, 3, 4 and 5.

Year	Total V (10^3 m^3)	Mean partial water volumes V_i (10^3 m^3)					Mean water velocity V_i (m/h)				
		FP1	FP2	FP3	FP4	FP5	FP1	FP2	FP3	FP4	FP5
1981	28.0	7.0	8.6	12.4	–	–	70.8	45.8	28.9		
1989	23.2	7.6	5.4	4.2	5.8	0.3	131.8	80.6	52.7	29.7	189.2

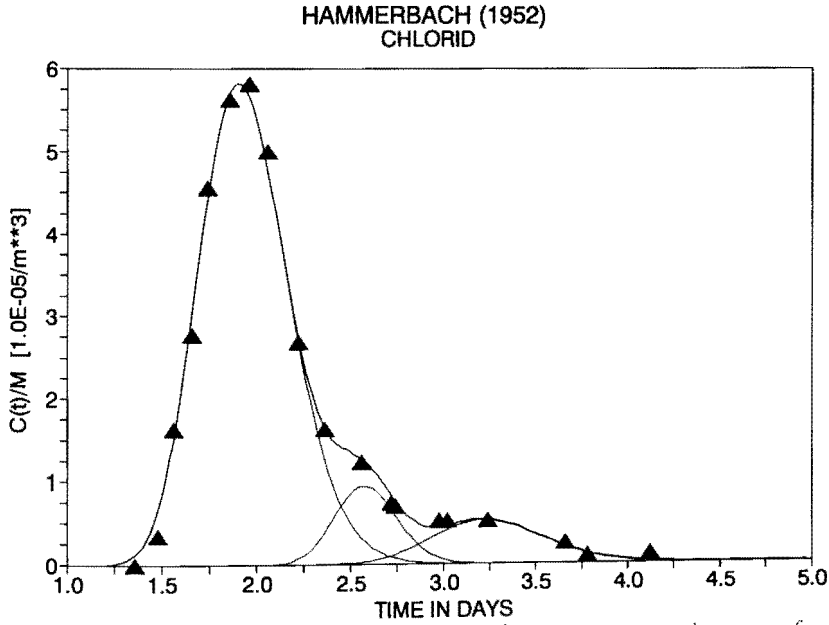

Fig. 6.3: The calculated (solid line) and observed (triangle) tracer concentration curves for the experiment performed in 1952 with chloride (dashed lines correspond to the partial curves).

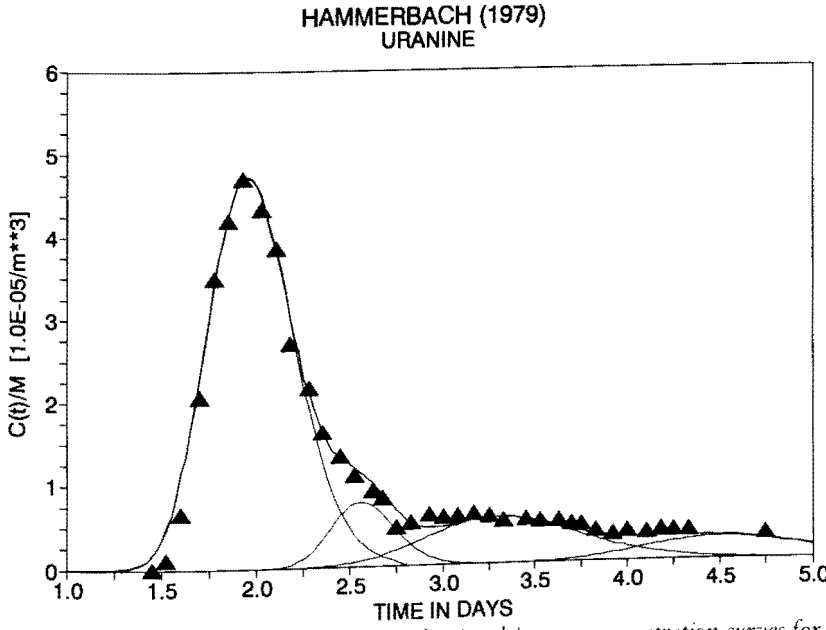

Fig. 6.4: The calculated (solid line) and observed (triangle) tracer concentration curves for the experiment performed in 1979 with uranine (dashed lines correspond to the partial curves).

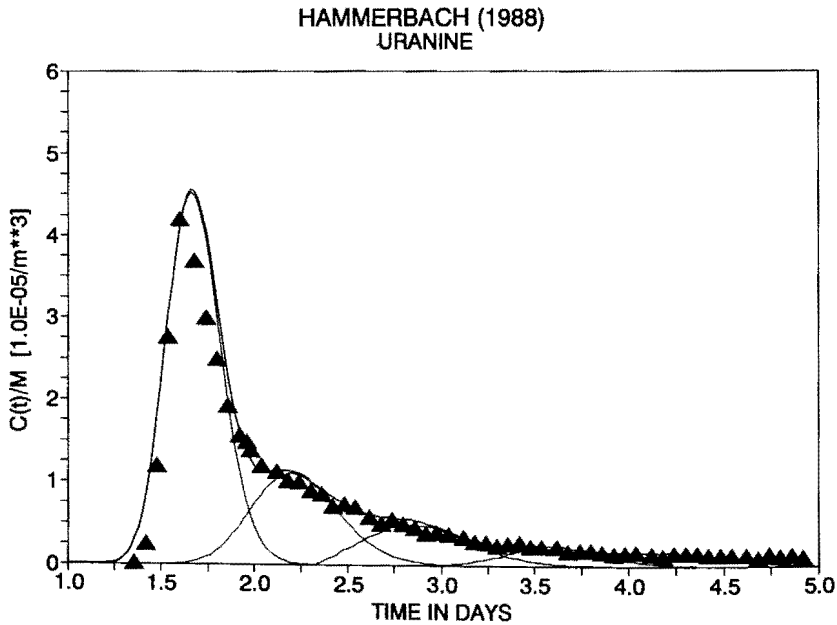

Fig. 6.5: The calculated (solid line) and observed (triangle) tracer concentration curves for the experiment performed in 1988 with uranine (dashed lines correspond to the partial curves).

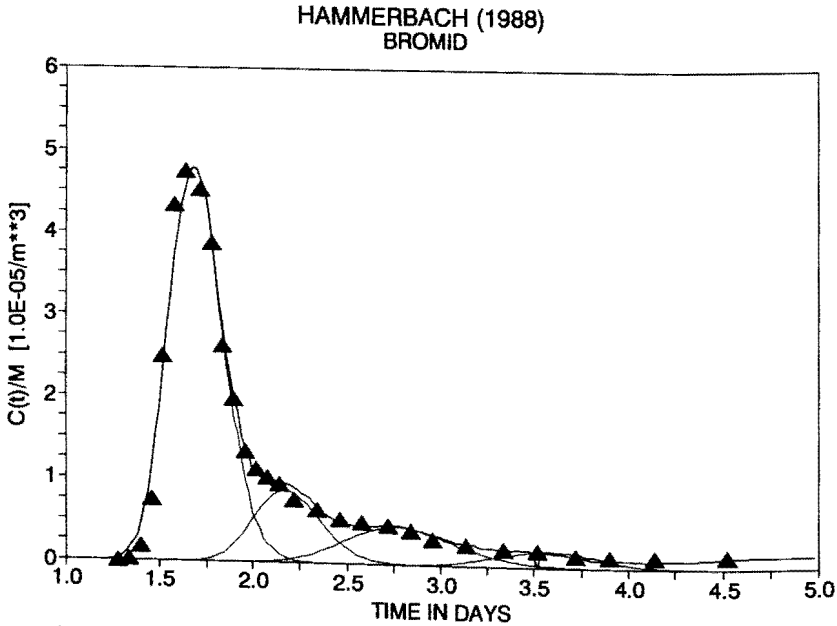

Fig. 6.6: The calculated (solid line) and observed (triangle) tracer concentration curves for the experiment performed in 1988 with bromide (dashed lines correspond to the partial curves).

6.1.4.2. Dispersivities

The dispersivities obtained for different flow paths are summarized in tab. 6.1. Table 6.7 includes their mean values. Figures 6.7–6.10 show a relatively low scatter of dispersivity values for different flow paths. This scatter increases from 10–25 m for the 1st flow path to 8–40 m for the 4th flow path. The mean values calculated separately for each flow path differ not so much (19.9–24.7 m). The dispersivities are generally independent from the discharge (s. fig. 6.7–6.10). The average value of all dispersivities is about 20 m.

Tab. 6.7: Mean dispersivities on the different flow paths and the average dispersivity for the Hammerbach and Schmelzbach systems. FP1, FP2, FP3, FP4 and FP5 = mean flow path 1, 2, 3, 4 and 5.

System	Dispersivity (m)					
	Total	FP1	FP2	FP3	FP4	FP5
Hammerbach	19.4	18.4	17.2	18.8	22.3	24.8
Schmelzbach	49.0	49.7	47.3	42.0		

6.1.4.3. Mean Transit Times

The mean transit times and water velocities vary very strongly but the general trend is that t_{0i} decreases (v_i increases) with increasing discharge Q (s. fig. 6.11). The mean transit time for the whole system is calculated as

$$t_0 = V/Q = \sum_{i=1}^{N} V_i/Q = \sum_{i=1}^{N} (r_i \cdot t_{0i}). \qquad (6.18)$$

6.1.4.4. Flow Rates and Volumes of Water

The portions of the tracer transported in each flow path, r_i, found from the tracer recoveries, were used to calculate the partial flow rates Q_i (s. tab. 6.2) and then, taking t_{0i}, to estimate the partial volumes of water V_i and the whole volume of water V in the system (s. tab. 6.3). Figures 6.12–6.14 show that V_i are nearly independent from the discharge Q. Figure 6.15 suggests that the total volume of water V may depend on the discharge Q for lower Q values. However all experiments with low discharges were finished too early and the additional flow paths could not be found. The rough approximation of the missing parts of the tracer breakthrough curves and reinterpretation of those experiments showed that the whole water volume V should be also considered as constant with rising discharge (s. fig. 6.15).

It seems that for the discharge variation between 80 and 400 l/s the whole drainage system is always saturated and has the total capacity for water limited to the volume of about 40×10^3 m^3. The arithmetic means of V_i calculated for different flow paths and their sums (understood as the maximum water volume in the system) are summarized in tab. 6.8.

The water volume in Schmelzbach system is estimated to be about 26×10^3 m^3. The whole drainage part of the karstic system between the Lurbach-sinkhole and the Hammerbach and Schmelzbach springs has about 65×10^3 m^3. The water volumes in the Hammerbach and Schmelzbach drainage systems are shown in fig. 6.16 and 6.17.

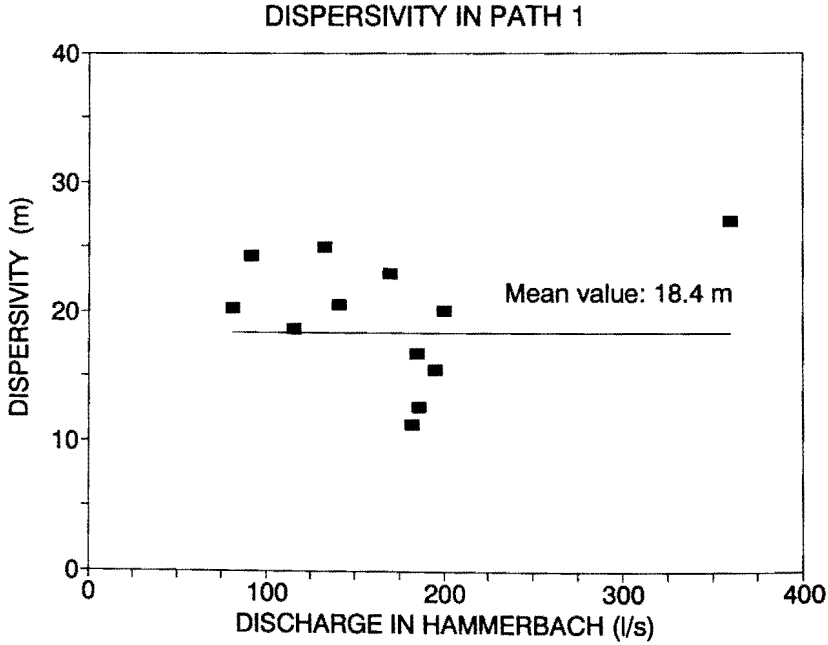

Fig. 6.7: Dispersivities α obtained for the 1st flow path in experiments with different discharge Q.

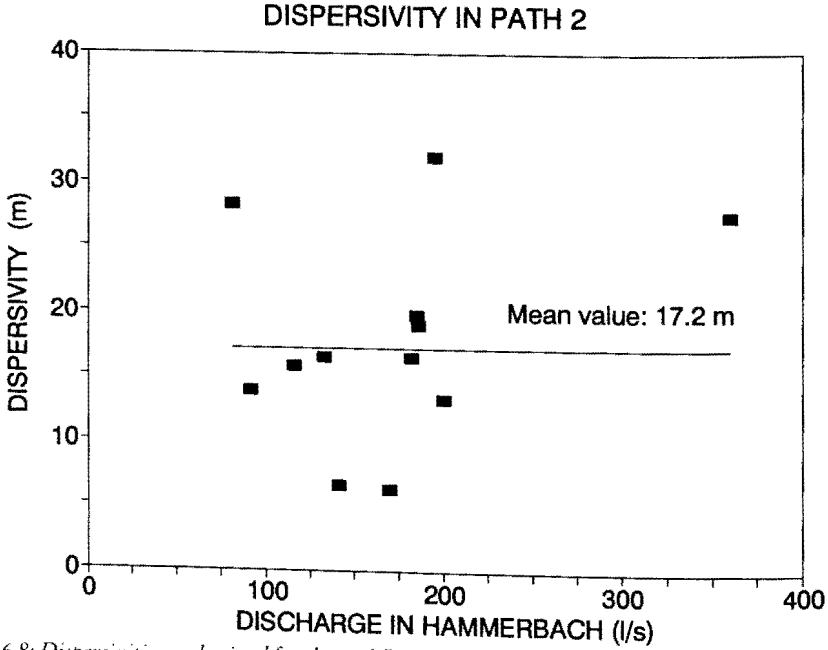

Fig. 6.8: Dispersivities α obtained for the 2nd flow path in experiments with different discharge Q.

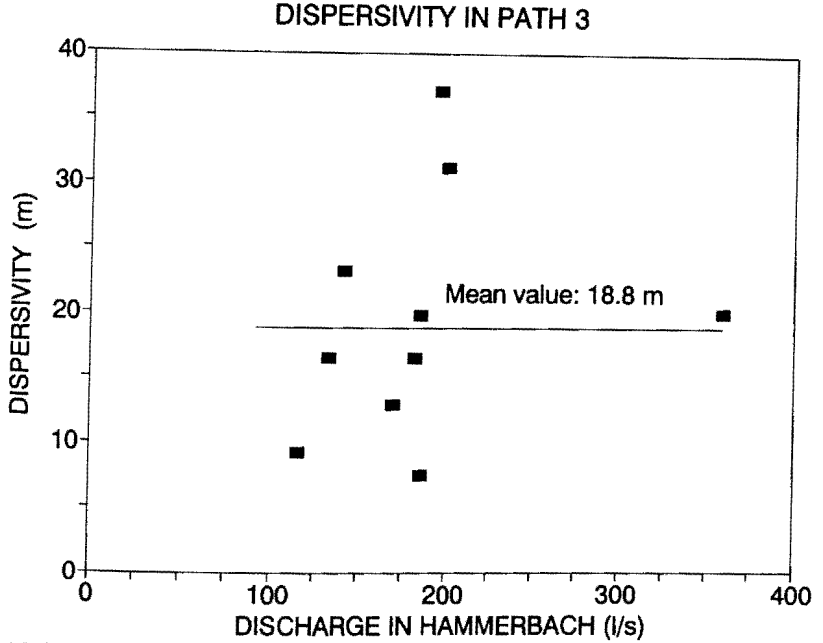

Fig. 6.9: Dispersivities α obtained for the 3th flow path in experiments with different discharge Q.

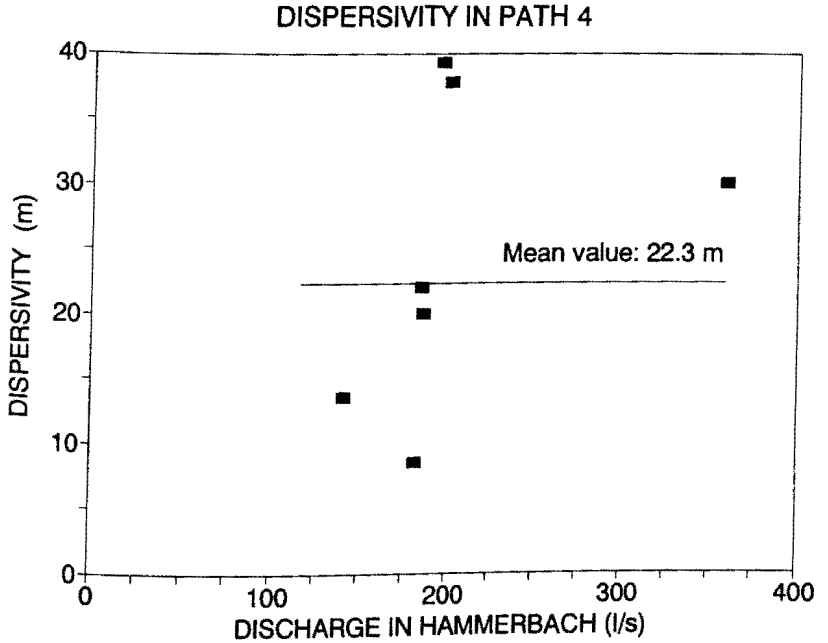

Fig. 6.10: Dispersivities α obtained for the 4th flow path in experiments with different discharge Q.

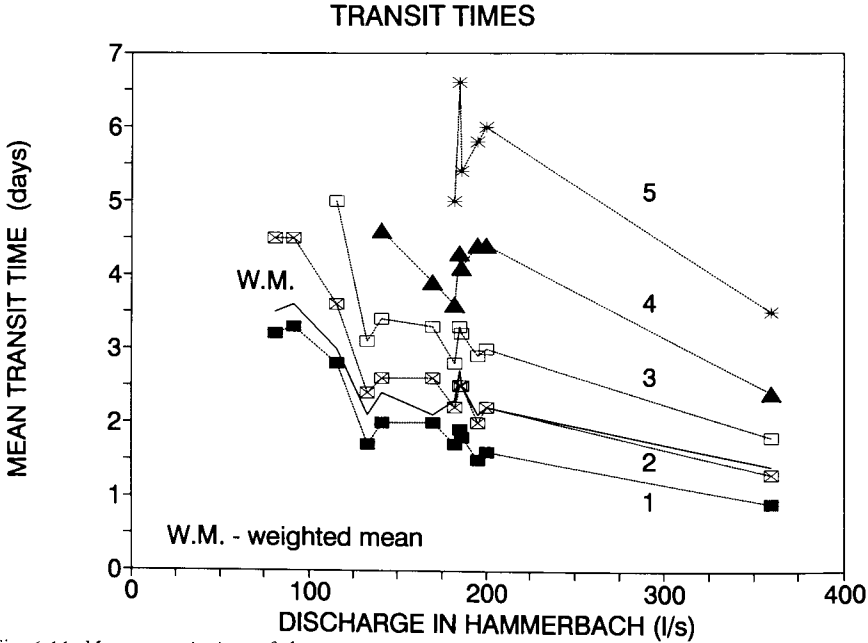

Fig. 6.11: Mean transit time of the Hammerbach system (solid line) and partial transit times on different flow paths as a function of discharge Q.

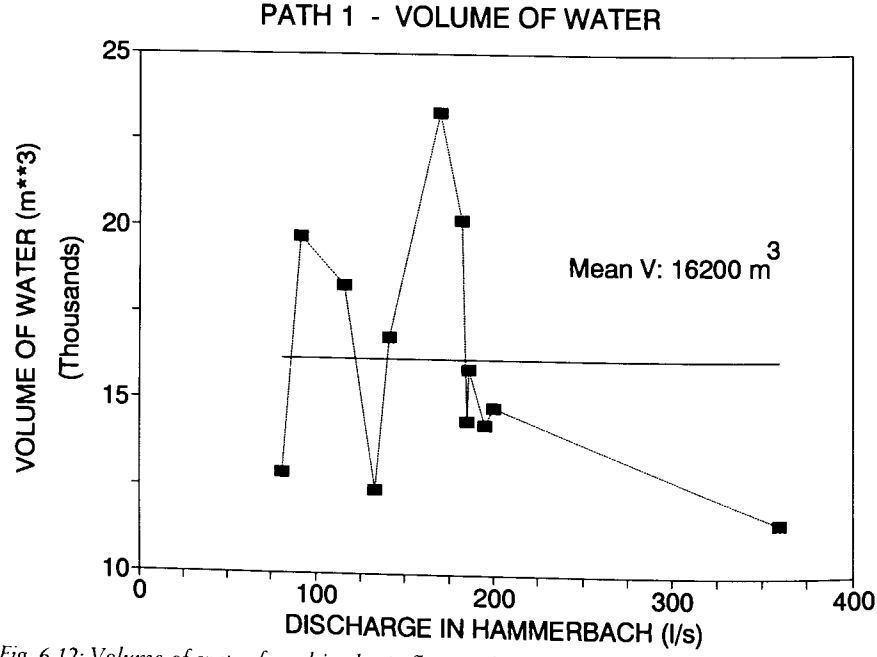

Fig. 6.12: Volume of water found in the 1st flow path of Hammerbach system as a function of discharge Q.

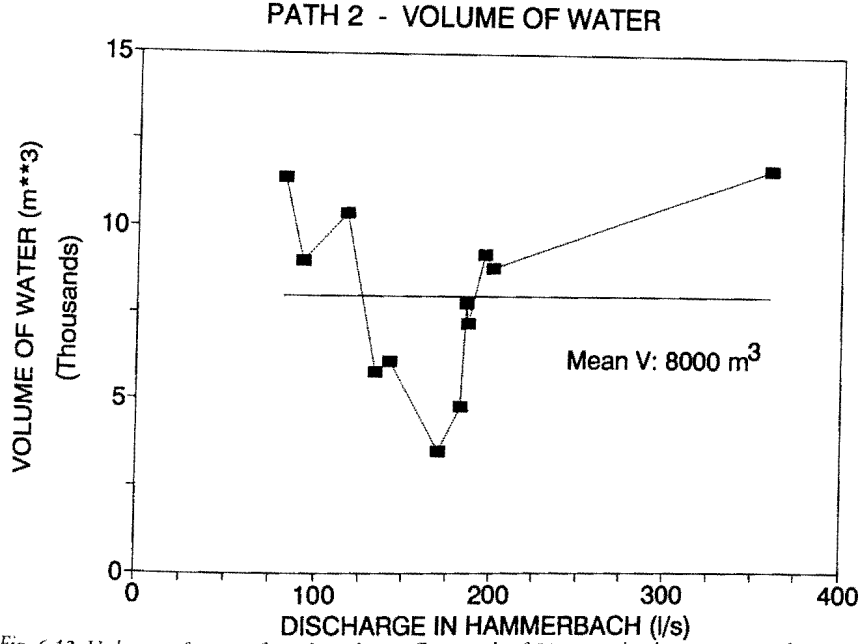

Fig. 6.13: Volume of water found in the 2nd flow path of Hammerbach system as a function of discharge Q.

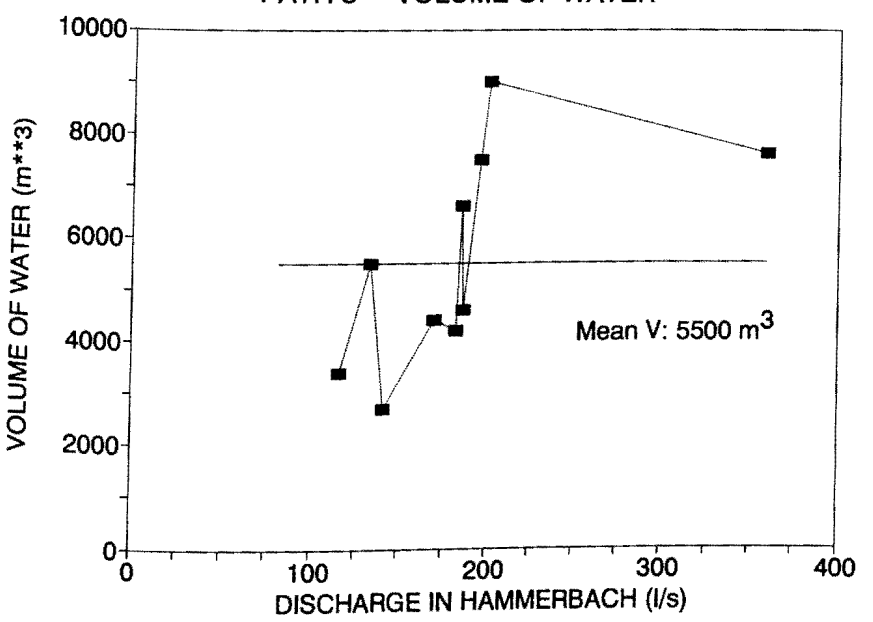

Fig. 6.14: Volume of water found in the 3th flow path of Hammerbach system as a function of discharge Q.

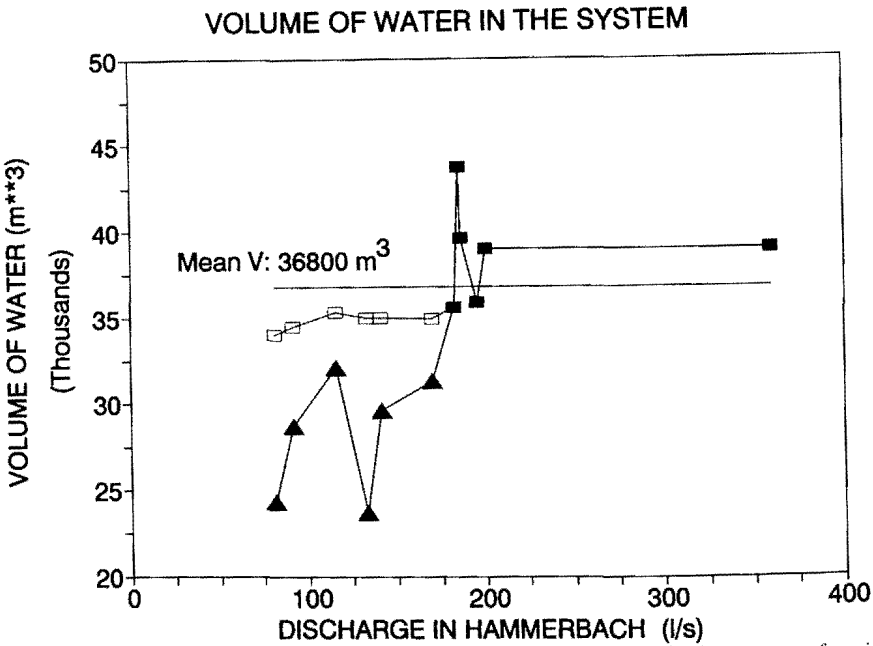

Fig. 6.15: The whole volume of water in the drainage channels of Hammerbach system as a function of discharge Q (triangles represent results from experiments which were finished to early; empty squares are estimated water volumes in those experiments).

Tab. 6.8: Maximum total and mean partial water volumes in drainage systems of Hammerbach and Schmelzbach. FP1, FP2, FP3, FP4 and FP5 = mean flow path 1, 2, 3, 4 and 5.

System	Volume of water in 10^3 m^3					
	Total(max)	FP1	FP2	FP3	FP4	FP5
Hammerbach	40.0	16.2	8.0	5.5	5.3	5.0
Schmelzbach	25.5	7.3	7.0	8.3	2.9	–

6.1.4.5. Prediction of Tracer Transport

The linear regression analysis applied to the Hammerbach system showed that the partial flow rates Q_i can with a satisfactory accuracy be estimated as a linear function of the total discharge Q:

$$Q_i = f(Q) = \beta_i \cdot Q \,. \qquad (6.19)$$

Results of the calculation of β_i for the four flow subsystems are shown in fig. 6.18–6.21 and agree well with the mean values of r_i found from individual experiments (Tab. 6.9).

As the system was found to be always saturated, eq. (6.19) gives the possibility to predict the mean transit time of water for single flow paths for different steady state flow conditions. Taking additionally into account nearly constant dispersivities for different flow paths, the model proposed in this study can be used to predict

HAMMERBACH

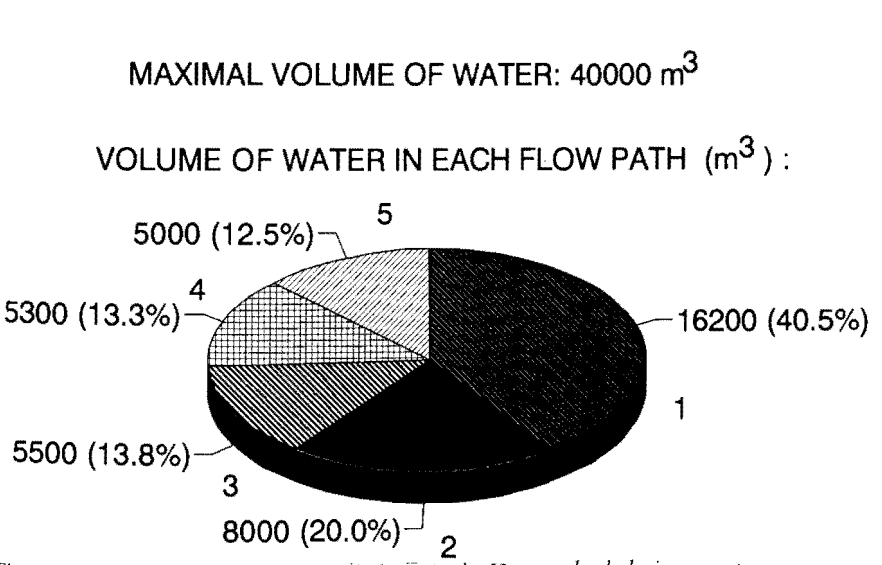

Fig. 6.16: Schematic diagram of water balance in the Hammerbach drainage system.

SCHMELZBACH

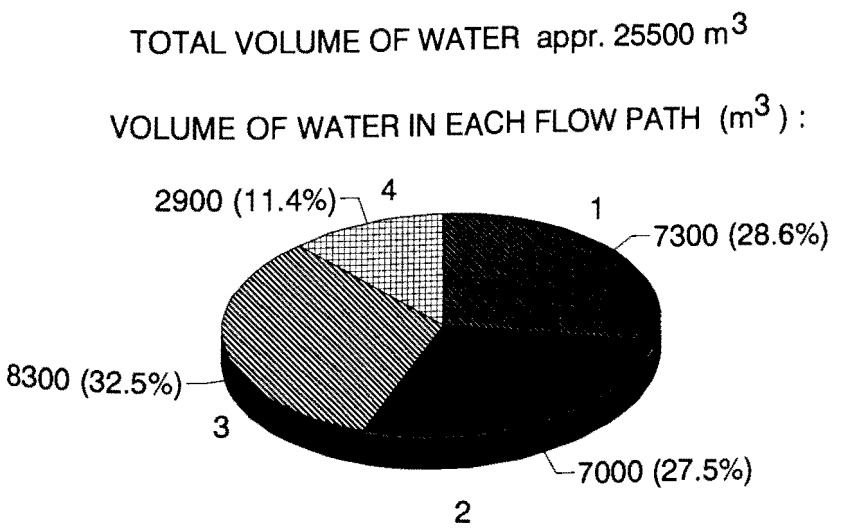

Fig. 6.17: Schematic diagram of water balance in the Schmelzbach drainage system.

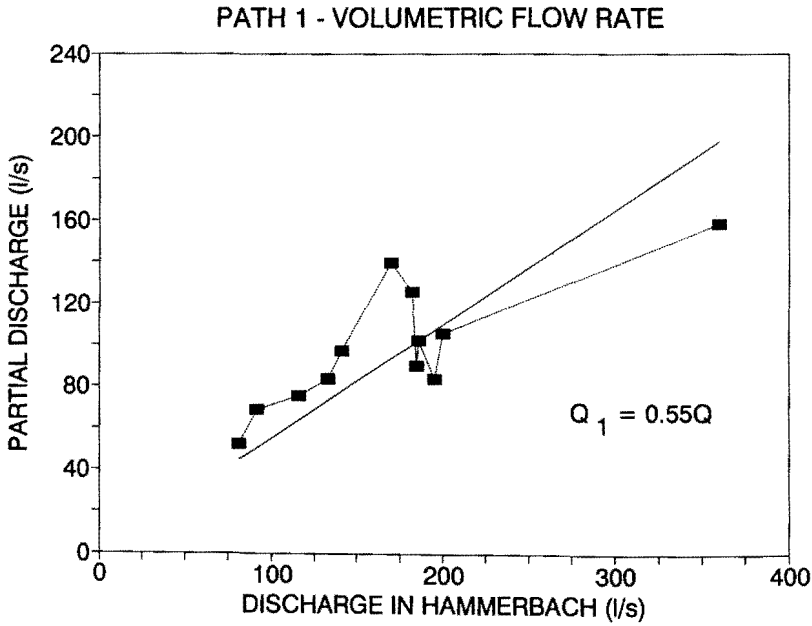

Fig. 6.18: Partial discharges in the 1st flow path as a function of the whole discharge $Q_1 = f(Q)$ approximated using linear regression.

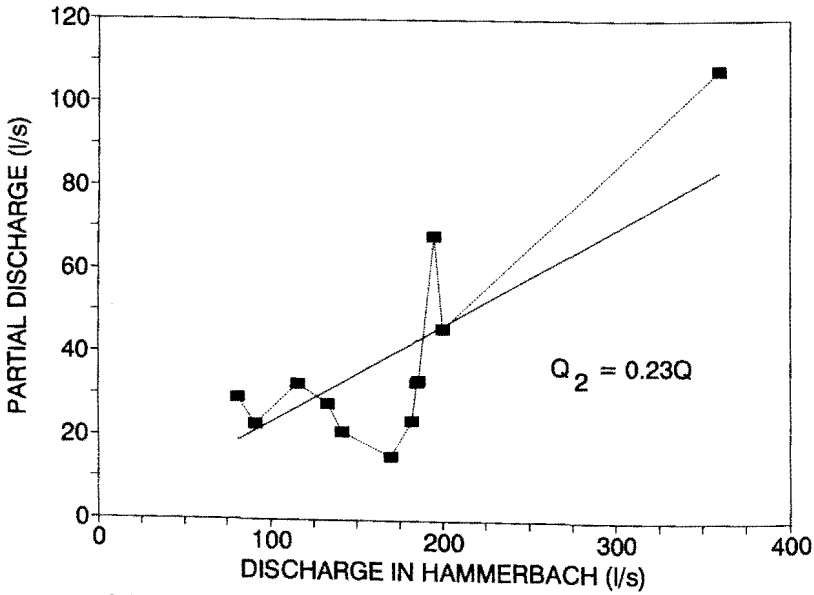

Fig. 6.19: Partial discharges in the 2nd flow path as a function of the whole discharge $Q_2 = f(Q)$ approximated using linear regression.

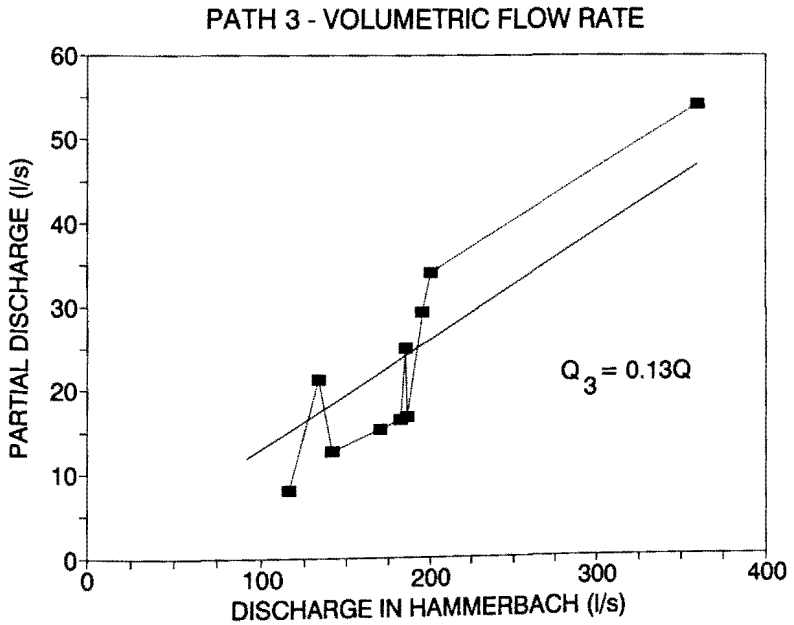

Fig. 6.20: Partial discharges in the 3th flow path as a function of the whole discharge $Q_3 = f(Q)$ approximated using linear regression.

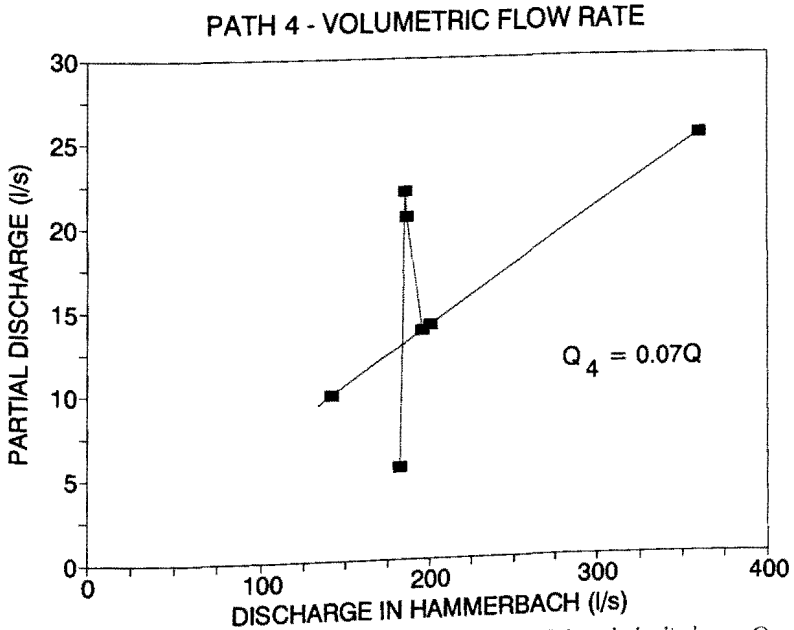

Fig. 6.21: Partial discharges in the 4th flow path as a function of the whole discharge $Q_4 = f(Q)$ approximated using linear regression.

Tab. 6.9: Mean portions of volumetric flow rates Q (discharge) flowing through different flow subsystems in drainage systems of Hammerbach and Schmelzbach. FP1, FP2, FP3, FP4 and FP5 = mean flow path 1, 2, 3, 4 and 5.

System	Portion of discharge in flow paths					
	Total	FP1	FP2	FP3	FP4	FP5
Hammerbach	1.0	0.55	0.22	0.12	0.07	0.04
Schmelzbach	1.0	0.45	0.27	0.21	0.06	0.01

the travel time of conservative solute (tracer or pollutant) in the Lurbach system for any state of steady flow, i.e. for any Q if this Q can be assumed as constant during the solute travel.

6.2. Modelling of Environmental Tracer Data

(P. MALOSZEWSKI, T. HARUM, H. ZOJER)

6.2.1. Introduction

The idea of the groundwater flow through a karstic catchment system was presented by R. BENISCHKE et al. (1988), K.-P. SEILER et al. (1989) and D. RANK et al. (1992) and is shown here in fig. 6.22. Generally, a karstic reservoir is approximated by two different flow systems.

The first system consists of a fissured-porous aquifer and has to be considered as a double porosity medium including mobile water flowing through the fissures and quasi stagnant water, or stagnant, in the microporous matrix. The surface of

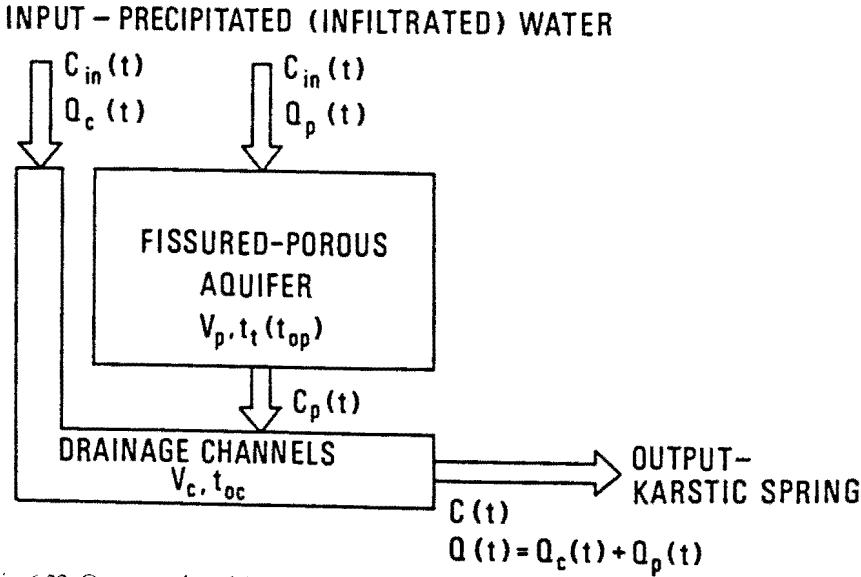

Fig. 6.22: Conceptual model of the water flow in the karstic catchment area (after D. RANK et al., 1992).

the system is in most cases the recharge zone of the catchment area. This system may be partially unsaturated and have a much greater storage volume than the second one. The tracer flow through this system is described by the dispersion-convection transport equation coupled with the diffusion term describing diffusive exchange of tracer between mobile and stagnant water (P. MALOSZEWSKI & A. ZUBER, 1984, 1991). The second system consists of the drainage channels. They can be connected directly with the surface of the catchment area through the sinkholes. The storage volume of this system is relatively small and the water flow very rapid. The tracer transport can be approximated by the piston flow model (taking into consideration the environmental tracer data) or by the dispersion model (for artificial tracer experiments).

The environmental tracer data were collected in the area under investigation mainly for a better understanding of the circulation of water in the system and for a quantitative estimation of the water storage volumes in different parts of the system. The mathematical modelling of the water flow through the drainage part of the system was performed on the basis of information obtained from the artificial tracer experiments described in detail in the previous chapter. This means that the drainage part of the system was considered as known for the modelling of environmental tracer data.

6.2.2. Basic Hydrologic Information

According to information given in chap. 2.3. the whole catchment area of Tanneben ($S_T = 22.8$ km^2) consists of schists of low permeability in the Lurbach catchment area ($S_{LB} = 14.5$ km^2) and of the karst massif of the Tanneben Plateau ($S_{PL} = 8.3$ km^2). The whole catchment area of Tanneben is drained by two karstic springs Hammerbach and Schmelzbach with the mean discharge $Q_{HB} = 192$ l/s and $Q_S = 97$ l/s, respectively.

Assuming that the whole groundwater system is closed (there is no underground water inflow or outflow) the mean yearly infiltration rate of $I = 400$ mm/a can be easily calculated from the sum of both discharges and the surface of the catchment area. For the mean annual precipitation equal to 900 mm/a it yields the mean evapotranspiration of about 500 mm/a which agrees reasonably with calculated 440 mm/a based on the classical method after TURC (s. chap. 2.3.6.).

Assuming the mean infiltration rate as constant on the whole surface of Tanneben, the volumetric flow rate of water infiltrating in the Tanneben Plateau and flowing through the karst massif into both springs is estimated to be $Q_{PL} = I \cdot S_{PL} = 105$ l/s. The water infiltrating through the surface of the Lurbach catchment area is collected by the Lurbach creek and inflows with $Q_{LB} = 184$ l/s (computed from the water balance equation, s. chap. 2.3.) directly through the sinkhole into the drainage channel systems of Hammerbach and Schmelzbach springs.

The mean discharge of each spring consists of two water components: first – Lurbach creek water, and second – water infiltrating in the Tanneben plateau and flowing through the karst massif.

6.2.3. Environmental Tracer Data

The measurements of the environmental tracer tritium were used to estimate water volumes in the karst massif of the Tanneben plateau and in the porous-fissured aquifer of the Lurbach catchment area. The tritium input function $C_{inp}(t)$ was calculated

for each year as a yearly weighted mean based on the simple infiltration model given by G.H. DAVIS et al. (1967):

$$C_{inp}(t) = \sum_{i=1}^{12} (P_i C_i \alpha_i) / \sum_{i=1}^{12} (P_i \alpha_i) , \qquad (6.20)$$

where P_i is the mean monthly precipitation amount, C_i the tritium content in precipitation and α_i the infiltration coefficient for the i-th month, respectively. It is assumed that the infiltration coefficients have the constant values α_S and α_W in two periods: summer (from April to September i = 4,9) and winter (from October to March i = 10,3), respectively, and that these values do not change from year to year. For the hydrological situation in the Tanneben catchment area the summer to winter infiltration coefficient was assumed $\alpha = \alpha_S/\alpha_W = 0.5$. J. GRABCZAK et al. (1984) have shown that if $\alpha \geq 0.4$, the result of modelling is nearly independent of the assumed value of α. The input function was calculated for the period 1950–1990 taking monthly precipitation amounts from the meteorological station of Frohnleiten (about 20 km to N in the Mur valley) and the tritium contents in precipitation for the Vienna station.

The output functions, $C_{out}(t)$ were the tritium concentrations in the water outflowing from different parts of the system: in the Lurbach creek at the sinkhole, in the Hammerbach and Schmelzbach springs and in a small spring (Laurins spring) in the vicinity of the Schmelzbach spring.

6.2.4. Mathematical Modelling

For the groundwater system being in a steady state (constant volumetric flow rate Q through the system and constant volume of water V in the system) the relation between input and output environmental tracer concentrations is given by the well known convolution integral (P. MALOSZEWSKI & A. ZUBER, 1982)

$$C_{out}(t) = \int_0^\infty C_{inp}(t-\tau)\, g(\tau) \exp(-\lambda\tau) d\tau , \qquad (6.21)$$

where λ is the radioactive decay constant (0.0564 a^{-1} for tritium) and $g(\tau)$ is the so-called weighting function or transit time distribution function which for the dispersion model is (P. MALOSZEWSKI & A. ZUBER, 1984):

$$g(\tau) = \frac{1}{\tau} \frac{1}{[4\pi (P_D)(\tau/t_t)]^{1/2}} \exp\left[-\frac{(1-\tau/t_t)^2}{4 (P_D)(\tau/t_t)}\right] , \qquad (6.22)$$

where t_t is the mean transit time of tracer and (P_D) is the artificial dispersion parameter describing the variance of the distribution of the transit times. Both parameters are the fitting parameters of the model. Their values are found by fitting the theoretical output concentrations calculated using eq. (6.21) with (6.22) to the tritium concentrations measured in the output.

In the saturated porous media, the mean transit time of tracer t_t is equal to the mean transit time of water:

$$t_0 = V_m/Q , \qquad (6.23)$$

where V_m is the volume of the mobile water in the system. In a karst massif considered as a double-porosity medium the mean transit time of tracer t_t can be used to estimate the total volume of water in the system (V_{tot}), i.e. the sum of the mobile

water in karstified fissures (V_m) and the stagnant water in the microporous rock matrix (V_{im})

$$t_t = V_{tot}/Q = (V_m + V_{im})/Q \,. \tag{6.24}$$

The above equation is valid only when the mean transit time of water is long enough (t_0 greater than about one year), see P. MALOSZEWSKI & A. ZUBER (1984). After determining the mean transit time of tracer (or water) from the environmental tracer data it is easy to find the volume of water in the system by applying eq. (6.23) or (6.24) for the known volumetric flow rate through the system Q. The surface of the catchment area (S), the mean total porosity (n), and the mean thickness of the aquifer (H) are related by:

$$H = Qt_t(Sn) \,. \tag{6.25}$$

6.2.5. Results of Modelling

The best fit of the theoretical tritium output curve to the concentrations measured in **Lurbach creek,** shown in fig. 6.23, was obtained with $(t_t)_{LB} = 4$ **a** and $(P_D)^* = 0.15$. By applying eq. (6.24) to the mean discharge of Lurbach creek $Q_{LB} = 184$ l/s it yields the mean total volume of water (stagnant and mobile) in this porous-fissured catchment area of about $V_{LB} = 23.2 \times 10^6$ m^3. For the aquifer thickness of 4–6 m and the catchment area of 14.5 km^2, the mean total porosity of weathered zone of schists calculated from eq. (6.25) is n = 0.3 which agrees well with the estimated from the geological data.

In both karstic springs the interpretation of tritium data is more complicated because the output concentrations result from mixing of two different flow components. The **Laurins spring** which collects water only from the karst massif (free of additional components) has shown the mean transit time of tracer of about 40 **a** (s. fig. 6.24). Unfortunately this spring is not representative for the whole karst massif. The total mean volumetric flow rate of water through the karst massif was estimated to be $Q_{PL} = 105$ l/s but this water flux is divided into two components $(Q_{PL})_{HB}$ and $(Q_{PL})_S$ of the Hammerbach and Schmelzbach springs, respectively. The artificial tracer experiments have shown that Schmelzbach water is free of the Lurbach creek water as long as the discharge of Hammerbach spring was lower than 200 l/s. This finding allows to calculate the mean discharge of Schmelzbach spring resulting from the infiltration of water into the Tanneben plateau $(Q_{PL})_S$ as equal to about 35 l/s. Consequently, the rest of water flux given as

$$(Q_{PL})_{HB} = Q_{PL} - (Q_{PL})_S = (105 - 35) = 70 \text{ l/s}$$

is the water flux through the karst massif flowing to the Hammerbach spring. The mean discharge in the Schmelzbach spring was $Q_S = 97$ l/s giving a portion of Lurbach creek water in this spring equal to

$$(Q_{LB})_S = Q_S - (Q_{PL})_S = (97 - 35) = 62 \text{ l/s} \,.$$

The portion of the Lurbach creek in the Hammerbach spring is then equal to

$$(Q_{LB})_{HB} = Q_{LB} - (Q_{LB})_S = (184 - 62) = 122 \text{ l/s} \,.$$

Taking into account tritium concentrations measured in the **Schmelzbach spring** only when the discharge of the Hammerbach spring was lower then 200 l/s, the mean

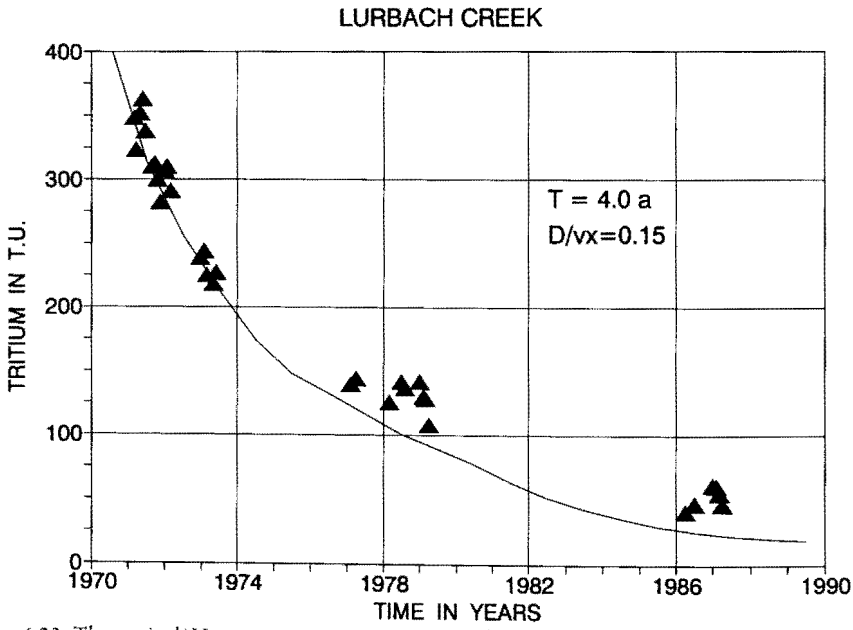

Fig. 6.23: Theoretical ^3H-output concentration curve obtained as the best fit to the concentrations measured during base flow conditions in the Lurbach creek.

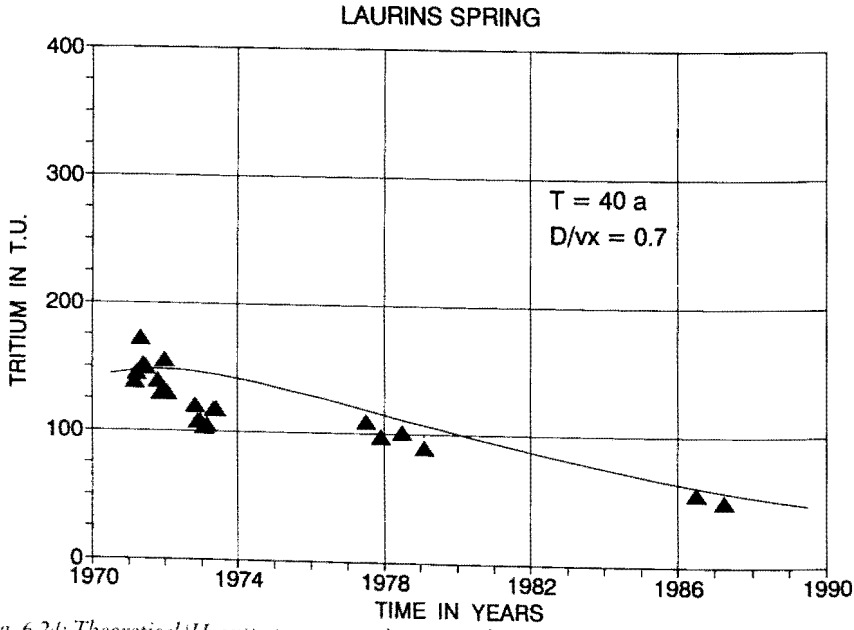

Fig. 6.24: Theoretical ^3H-output concentration curve obtained as the best fit to the concentrations measured in the Laurins spring (Schmelzbach system).

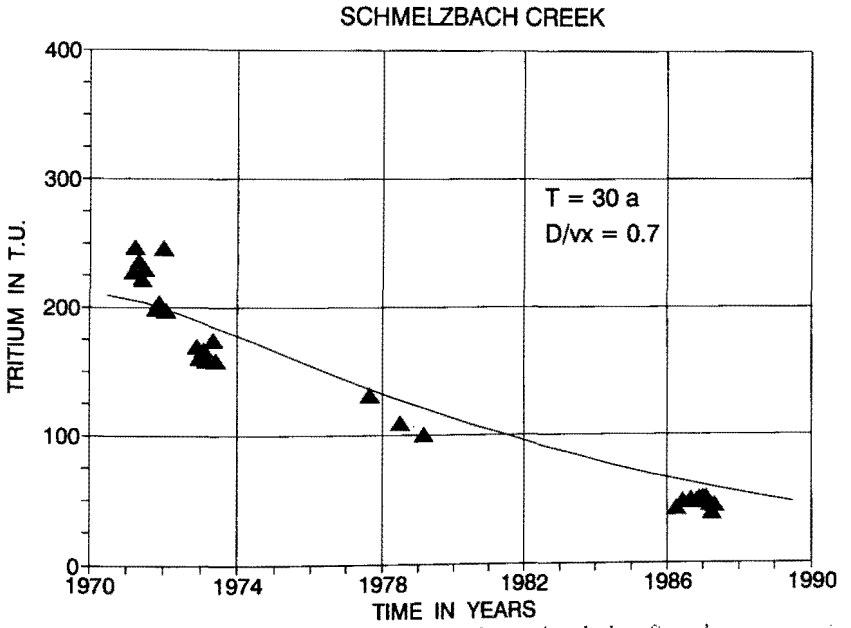

Fig. 6.25: Theoretical ^3H-output concentration curve obtained as the best fit to the concentrations measured during low flow conditions in the Schmelzbach spring (free of Lurbach component).

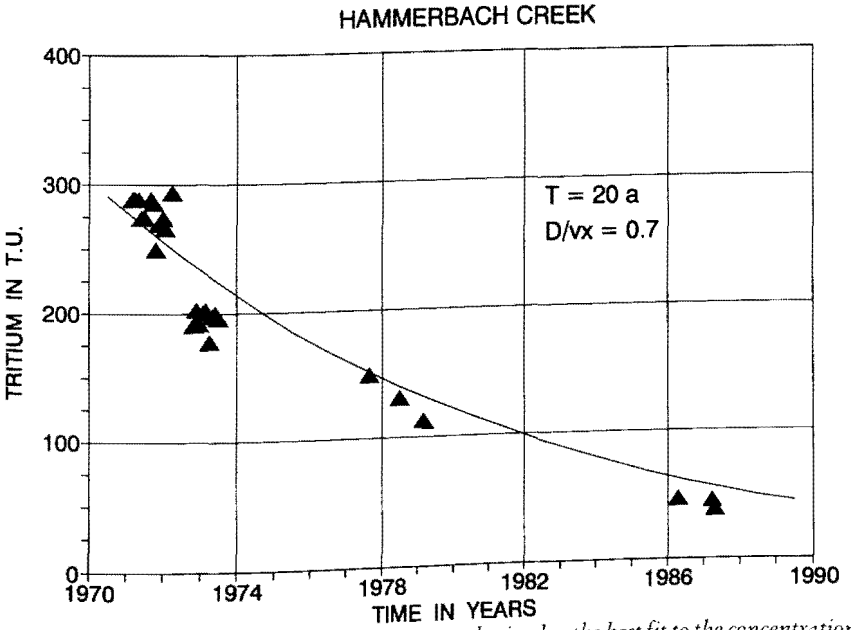

Fig. 6.26: Theoretical ^3H-output concentration curve obtained as the best fit to the concentrations measured during base flow conditions in the Hammerbach spring.

transit time of tracer equal to **30 a** was found (s. fig. 6.25). It shows that the discharge of the Schmelzbach spring – which is draining the part of the karst massif like the Laurins spring – has even at low flow conditions (i.e. without connection to the Hammerbach system) a younger water component than the Laurins spring. This younger component probably consists of water from the two sinkholes Katzenbach and Eisgrube their connection with the Schmelzbach spring being proved by tracing experiments (s. chap. 5.2.).

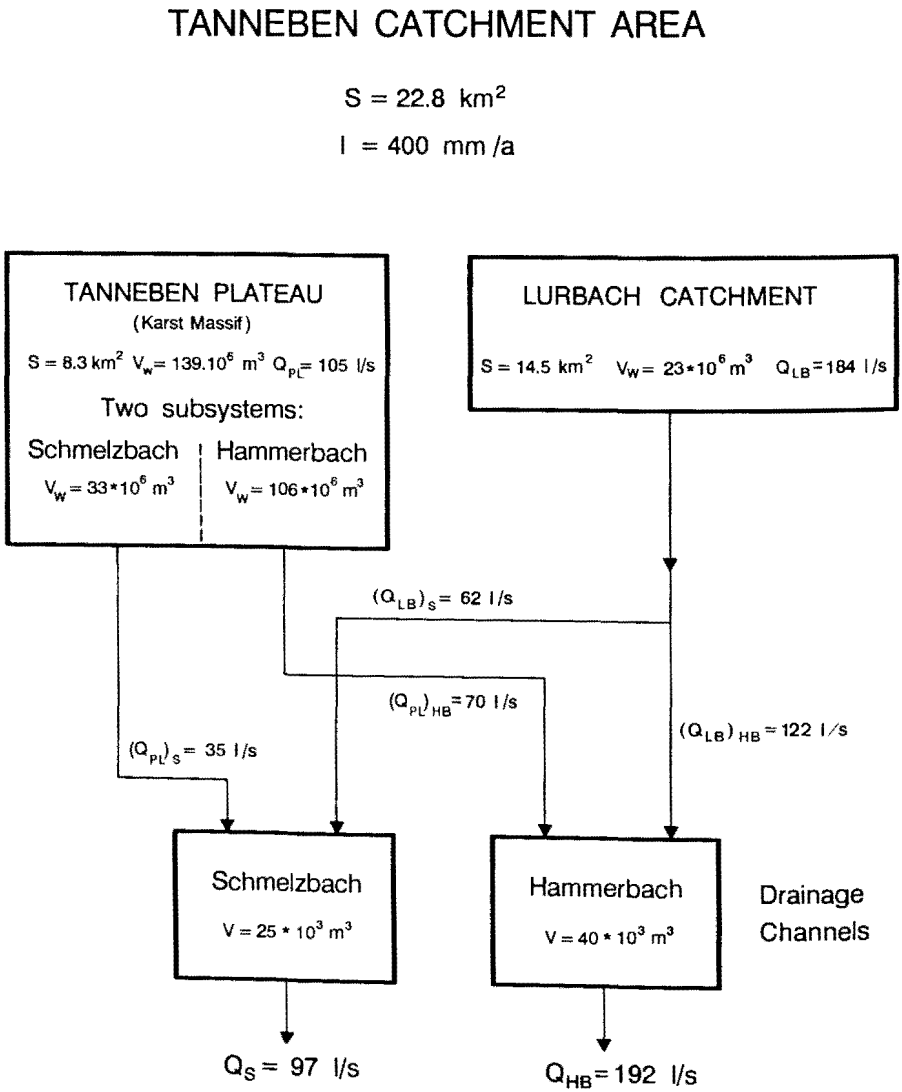

Fig. 6.27: The reservoir features of the Tanneben karstic catchment basin found using artificial and environmental tracer data (s. text).

The volume of water in the system observed from the Schmelzbach spring was then calculated to be

$$(V_{PL})_S = 33.1 \times 10^6 \text{ m}^3 .$$

In the **Hammerbach spring** the mixing of two components (Lurbach and karst massif water) is permanently observed. The mean transit time of tritium found there was equal to **20 a** (the best fit curve is shown in fig. 6.26). Assuming the good mixing of water in the spring, the mean transit time is the weighted mean value of the transit times of two water components

$$(t_t)_{HB} = [(Q_{LB})_{HB} \cdot (t_t)_{LB} + (Q_{PL})_{HB} \cdot (t_t)_{PLHB}]/Q_{HB} . \qquad (6.26)$$

After rearrangements the mean transit time of water component flowing through the karst massif to the Hammerbach spring is

$$(t_t)_{PLHB} = [(t_t)_{HB} \cdot Q_{HB} - (Q_{LB})_{HB} \cdot (t_t)_{LB}]/(Q_{PL})_{HB} . \qquad (6.27)$$

Putting $(t_t)_{HB} = 20$ a, $(t_t)_{LB} = 4$ a, $Q_{HB} = 192$ l/s, $(Q_{LB})_{HB} = 122$ l/s and $(Q_{PL})_{HB} = 70$ l/s one obtains finally **$(t_t)_{PLHB} = 48$ a**. It yields from eq. (6.24) the volume of water in the karst massif system of the Hammerbach spring **$(V_{PL})_{HB}$, equal to 106×10^6 m³. The total volume of water in the karst massif V_{PL}, the sum of $(V_{PL})_{HB}$ and $(V_{PL})_S$, is about 139×10^6 m³.** For the mean thickness of karst massif of 340 m the **total porosity of 4.9%** (water saturated – mobile and stagnant) can be estimated from eq. (6.25).

Finally, it is interesting to point out that the ratio of water fluxes through the karst massif to the water fluxes through the drainage channels was nearly 1 : 2 (105 : 184), whereas the ratio of the water volumes in the karst massif to the water volumes in the drainage channels was about 2,000 : 1 (139,000 : 65). Figure 6.27 shows the conceptual model with the values of water fluxes and water storage volumes in the area under investigation.

7. Summary and Conclusions

7.1. General Remarks (H. ZOJER)

The common use of environmental and artificial tracer methods has been incorporated into the concept of karst water research in the investigated area. It shows very clearly, that tracer studies are important adjuncts to other more conventional methods. All these considerations lead to their methodological application in two main fields of karst hydrogeology, the calculation of subsurface water storage and the localization of recharge areas of springs and wells. In this reference quantitative aspects in karst hydrogeology can be obtained in creating tracer models expressed as a mass transport.

The results of artificial tracing experiments on the one hand and environmental tracer studies on the other simulate some contradictions, since tracers are usually injected at locations with a quick water input from the surface. This gives the impression of a short subsurface turnover time, but not representing the general infiltration conditions in the total recharge area. The environmental tracers on the other hand, measured at the outlets of the system, refer to the whole drainage and